

UFIFT-QG-16-08 , CCTP-2016-10
CCQCN-2016-147 , ITCP-IPP 2016/08

Final Thoughts on the Power Spectra of Scalar Potential Models

D. J. Brooker^{1*}, N. C. Tsamis²⁺ and R. P. Woodard^{1†}

¹ *Department of Physics, University of Florida,
Gainesville, FL 32611, UNITED STATES*

² *Institute of Theoretical Physics & Computational Physics,
Department of Physics, University of Crete,
GR-710 03 Heraklion, HELLAS*

ABSTRACT

We give final shape to a recent formalism for deriving the functional forms of the primordial power spectra of single-scalar potential models and theories which are related to them by conformal transformation. An excellent analytic approximation is derived for the nonlocal correction factors which are crucial to capture the “ringing” that can result from features in the potential. We also present the full algorithm for using our representation, including the nonlocal factors, to reconstruct the inflationary geometry from the power spectra.

PACS numbers: 04.50.Kd, 95.35.+d, 98.62.-g

* e-mail: djbrooker@ufl.edu

+ e-mail: tsamis@physics.uoc.gr

† e-mail: woodard@phys.ufl.edu

1 Introduction

The simplest models of primordial inflation are based on general relativity (for a spacelike metric $g_{\mu\nu}(x)$) plus a single, minimally coupled scalar $\varphi(x)$,

$$\mathcal{L} = \frac{R\sqrt{-g}}{16\pi G} - \frac{1}{2}\partial_\mu\varphi\partial_\nu\varphi g^{\mu\nu}\sqrt{-g} - V(\varphi)\sqrt{-g}. \quad (1)$$

A key prediction is the generation of tensor [1] and scalar [2] perturbations. These are the first observable quantum gravitational phenomena ever recognized as such [3, 4, 5]. They are also our chief means of testing the viability of scalar potential models [6, 7, 8], and of reconstructing $V(\varphi)$ [9, 10, 11].

Reconstruction is simplest in terms of the Hubble representation [12] using the Hubble parameter $H(t)$ and first slow roll parameter $\epsilon(t)$ of the homogeneous, isotropic and spatially flat background geometry of inflation,¹

$$ds^2 = -dt^2 + a^2(t)d\vec{x}\cdot d\vec{x} \implies H(t) \equiv \frac{\dot{a}}{a} > 0 \quad , \quad \epsilon(t) \equiv -\frac{\dot{H}}{H^2} < 1. \quad (2)$$

Let t_k stand for the time of first horizon crossing, when modes of wave number k obey $k \equiv H(t_k)a(t_k)$. The tensor and scalar power spectra take the form of leading slow roll results at $t = t_k$, multiplied by local slow roll corrections also at $t = t_k$, times nonlocal factors involving times near $t = t_k$ [18, 19],

$$\Delta_h^2(k) = \frac{16}{\pi}GH^2(t_k) \times C(\epsilon(t_k)) \times \exp\left[\tau[\epsilon](k)\right], \quad (3)$$

$$\Delta_{\mathcal{R}}^2(k) = \frac{GH^2(t_k)}{\pi\epsilon(t_k)} \times C(\epsilon(t_k)) \times \exp\left[\sigma[\epsilon](k)\right]. \quad (4)$$

The local slow roll correction $C(\epsilon)$ is,

$$C(\epsilon) \equiv \frac{1}{\pi}\Gamma^2\left(\frac{1}{2} + \frac{1}{1-\epsilon}\right) \left[2(1-\epsilon)\right]^{\frac{2}{1-\epsilon}} \approx 1 - \epsilon. \quad (5)$$

The nonlocal correction exponents, $\tau[\epsilon](k)$ and $\sigma[\epsilon](k)$, vanish for $\dot{\epsilon} = 0$ and effectively depend on the geometry only a few e-foldings before and after t_k [18, 19].

¹The connection to the potential representation is [13, 14, 15, 16, 17],

$$\varphi_0(t) = \varphi_0(t_i) \pm \int_{t_i}^t dt' H(t') \sqrt{\frac{\epsilon(t')}{4\pi G}} \iff t(\varphi) \quad , \quad V(\varphi) = \frac{[3-\epsilon(t)]H^2(t)}{8\pi G} \Big|_{t=t(\varphi)}.$$

The purpose of this paper is to rationalize and simplify our formalism for evolving the norms of the mode functions, rather than the mode functions [20], and then to derive an excellent analytic approximation for the nonlocal correction exponents $\tau[\epsilon](k)$ and $\sigma[\epsilon](k)$. We also demonstrate how this approximation can be used to reconstruct the inflationary geometry from the power spectra, even for models which possess features. These topics represent sections 2-3, 4 and 5, respectively. In section 6 we discuss some of the many applications [21, 22] this formalism facilitates.

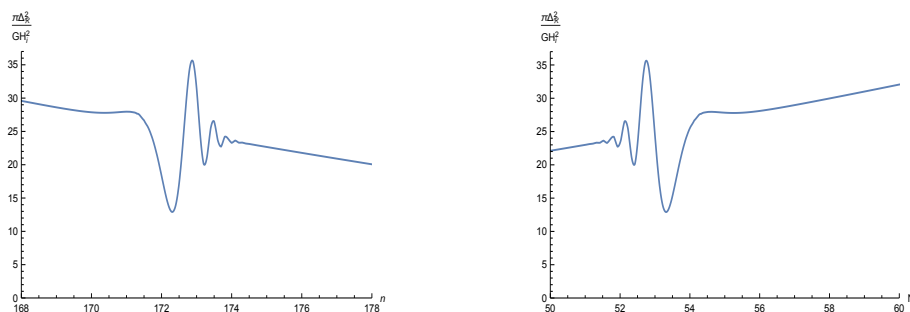


Figure 1: The left hand graph shows one model's scalar power spectrum as a function of n , the number of e-foldings from the beginning of inflation to first horizon crossing. The right hand graph shows the same power spectrum versus N , the number of e-foldings *until* the end of inflation. Early times correspond to small n and large N , whereas late times correspond to large n and small N .

We shall often employ the alternate time parameter provided by $n \equiv \ln[a(t)/a_i]$, the number of e-foldings since inflation's onset. This is superior to the co-moving time t by virtue of being dimensionless and relating evolution to the size of the universe. We shall abuse the notation slightly by writing $H(n)$ and $\epsilon(n)$, instead of the correct but cumbersome expressions $H(t(n))$ and $\epsilon(t(n))$. Which time parameter pertains should be clear from context, and from our exclusive use of ℓ , m and n to stand for e-foldings. Over-dots represent time derivatives and primes stand for n derivatives,

$$\epsilon = -\frac{\dot{H}}{H^2} = -\frac{H'}{H} \iff H = \frac{H_i}{1 + \int_{t_i}^t dt' \epsilon(t')} = H_i \exp\left[-\int_0^n dm \epsilon(m)\right]. \quad (6)$$

We caution readers against confusing n with the common parameter $N \equiv n_e - n$, the number of e-foldings until the end of inflation (at $n = n_e$). Figure 1 illustrates the difference.

2 Our Formalism in General

The tree order tensor power spectrum is obtained by evolving the graviton mode function $u(t, k)$ past the time of first horizon crossing [9, 10, 11],

$$\Delta_h^2(k) = \frac{k^3}{2\pi^2} \times 32\pi G \times 2 \times \lim_{t \gg t_k} \left| u(t, k) \right|^2. \quad (7)$$

We do not possess exact solutions for $u(t, k)$ for realistic geometries $\epsilon(t)$, but we do know the evolution equation, the Wronskian and the form at asymptotically early times [9, 10, 11, 23],

$$\ddot{u} + 3H\dot{u} + \frac{k^2}{a^2}u = 0 \quad , \quad u\dot{u}^* - \dot{u}u^* = \frac{i}{a^3} \quad , \quad u(t, k) \longrightarrow \frac{\exp[-ik \int_{t_i}^t \frac{dt'}{a(t')}]}{\sqrt{2ka^2(t)}}. \quad (8)$$

Because the power spectrum depends upon the norm-squared, rather than the rapidly-varying phase, it is better to convert (8) into a nonlinear evolution equation for $M(t, k) \equiv |u(t, k)|^2$ [20],

$$\ddot{M} + 3H\dot{M} + \frac{2k^2}{a^2}M = \frac{1}{2M} \left(\dot{M}^2 + \frac{1}{a^6} \right) \quad , \quad M(t, k) \longrightarrow \frac{1}{2ka^2(t)}. \quad (9)$$

If necessary, the mode function can be easily recovered [19],

$$u(t, k) = \sqrt{M(t, k)} \exp \left[-\frac{i}{2} \int_{t_i}^t \frac{dt'}{a^3(t')M(t', k)} \right]. \quad (10)$$

Relation (9) can be improved by changing to the dimensionless time parameter $n = \ln[a(t)/a_i]$,

$$\left(\frac{M'}{M} \right)' + \frac{1}{2} \left(\frac{M'}{M} \right)^2 + (3-\epsilon) \frac{M'}{M} + \frac{2k^2}{H^2 a^2} - \frac{1}{2H^2 a^6 M^2} = 0. \quad (11)$$

A further improvement comes by factoring out an (at this stage) arbitrary approximate solution, $M_0(t, k)$, to derive a damped, driven oscillator equation (with small nonlinearities) for the residual exponent [18],

$$M = M_0 \times e^{-\frac{1}{2}h} \quad \implies \quad h'' - \frac{\omega'}{\omega} h' + \omega^2 h = S_h + \frac{1}{4} h'^2 - \omega^2 [e^h - 1 - h]. \quad (12)$$

Here the frequency $\omega(n, k)$ and the tensor source $S_h(n, k)$ are,

$$\omega \equiv \frac{1}{Ha^3 M_0} \implies S_h = -2 \left(\frac{\omega'}{\omega} \right)' + \left(\frac{\omega'}{\omega} \right)^2 + 2\epsilon' - (3 - \epsilon)^2 + \frac{4k^2}{H^2 a^2} - \omega^2. \quad (13)$$

It is an amazing fact that an exact Green's function exists for the left hand side of equation (12), valid for *any* choice of the approximate solution M_0 [18],

$$G_h(n; m) = \frac{\theta(n-m)}{\omega(m, k)} \sin \left[\int_0^n d\ell \omega(\ell, k) \right]. \quad (14)$$

This permits us to solve (12) perturbatively $h = h_1 + h_2 + \dots$ by expanding in the nonlinear terms,

$$h_1(n, k) = \int_0^n dm G_h(n; m) S_h(m, k), \quad (15)$$

$$h_2(n, k) = \int_0^n dm G_h(n; m) \left\{ \frac{1}{4} \left[h_1'(m, k) \right]^2 - \frac{1}{2} \left[\omega(m, k) h_1(m, k) \right]^2 \right\}. \quad (16)$$

The tree order scalar power spectrum is obtained by evolving the ζ mode function $v(t, k)$ past the time of first horizon crossing [9, 10, 11],

$$\Delta_{\mathcal{R}}^2(k) = \frac{k^3}{2\pi^2} \times 4\pi G \times \lim_{t \gg t_k} \left| v(t, k) \right|^2. \quad (17)$$

Just as for its tensor cousin, we lack exact solutions for $v(t, k)$ for realistic geometries $\epsilon(t)$, but we do know the evolution equation, the Wronskian and the form at asymptotically early times [9, 10, 11, 23],

$$\ddot{v} + \left(3H + \frac{\dot{\epsilon}}{\epsilon} \right) \dot{v} + \frac{k^2}{a^2} v = 0, \quad v\dot{v}^* - \dot{v}v^* = \frac{i}{\epsilon a^3}, \quad v(t, k) \longrightarrow \frac{\exp[-ik \int_{t_i}^t \frac{dt'}{a(t')}] }{\sqrt{2k\epsilon(t)a^2(t)}}. \quad (18)$$

Converting to the norm-squared $\mathcal{N}(t, k) \equiv |v(t, k)|^2$ gives [19],

$$\ddot{\mathcal{N}} + \left(3H + \frac{\dot{\epsilon}}{\epsilon} \right) \dot{\mathcal{N}} + \frac{2k^2}{a^2} \mathcal{N} = \frac{1}{2\mathcal{N}} \left(\dot{\mathcal{N}}^2 + \frac{1}{\epsilon^2 a^6} \right), \quad \mathcal{N}(t, k) \longrightarrow \frac{1}{2k\epsilon(t)a^2(t)}. \quad (19)$$

The scalar mode function mode can be recovered from $\mathcal{N}(t, k)$ [19],

$$v(t, k) = \sqrt{\mathcal{N}(t, k)} \exp \left[-\frac{i}{2} \int_{t_i}^t \frac{dt'}{\epsilon(t')a^3(t')\mathcal{N}(t', k)} \right]. \quad (20)$$

Converting from co-moving time t to $n = \ln[a(t)/a_i]$ gives,

$$\left(\frac{\mathcal{N}'}{\mathcal{N}}\right)' + \frac{1}{2}\left(\frac{\mathcal{N}'}{\mathcal{N}}\right)^2 + \left(3 - \epsilon + \frac{\epsilon'}{\epsilon}\right)\frac{\mathcal{N}'}{\mathcal{N}} + \frac{2k^2}{H^2 a^2} - \frac{1}{2\epsilon^2 H^2 a^6 \mathcal{N}^2} = 0. \quad (21)$$

Factoring out by an arbitrary approximate solution $\mathcal{N}_0(t, k)$ produces another damped, driven oscillator equation for the residual exponent,

$$\mathcal{N} = \mathcal{N}_0 \times e^{-\frac{1}{2}g} \implies g'' - \frac{\Omega'}{\Omega}g' + \Omega^2 g = S_g + \frac{1}{4}g'^2 - \Omega^2 [e^g - 1 - g]. \quad (22)$$

Here the frequency $\Omega(n, k)$ and the scalar source $S_g(n, k)$ are,

$$\Omega \equiv \frac{1}{\epsilon H a^3 \mathcal{N}_0}, \quad (23)$$

$$S_g = -2\left(\frac{\Omega'}{\Omega}\right)' + \left(\frac{\Omega'}{\Omega}\right)^2 + 2\epsilon' - \left(3 - \epsilon + \frac{\epsilon'}{\epsilon}\right)^2 - 2\left(\frac{\epsilon'}{\epsilon}\right)' + \frac{4k^2}{H^2 a^2} - \Omega^2. \quad (24)$$

Making the replacement $\omega \rightarrow \Omega$ in (14) gives an exact Green's function which is valid for any choice of \mathcal{N}_0 ,

$$G_g(n; m) = \frac{\theta(n-m)}{\Omega(m, k)} \sin \left[\int_0^n d\ell \Omega(\ell, k) \right]. \quad (25)$$

And we can of course develop a perturbative solution to (22) $g = g_1 + g_2 + \dots$,

$$g_1(n, k) = \int_0^n dm G_g(n; m) S_g(m, k), \quad (26)$$

$$g_2(n, k) = \int_0^n dm G_g(n; m) \left\{ \frac{1}{4} [g_1'(m, k)]^2 - \frac{1}{2} [\Omega(m, k) g_1(m, k)]^2 \right\}. \quad (27)$$

3 Choosing $M_0(t, k)$ and $\mathcal{N}_0(t, k)$ Effectively

The formalism of the previous section is valid for all choices of the approximate solutions $M_0(t, k)$ and $\mathcal{N}_0(t, k)$. Of course the correction exponents $h(n, k)$ and $g(n, k)$ will be smaller if the zeroth order solutions are more carefully chosen. In previous work we used the instantaneously constant ϵ solutions [18, 19],

$$M_{\text{inst}}(t, k) \equiv \frac{z(t, k) \mathcal{H}(\nu(t), z(t, k))}{2ka^2(t)}, \quad \mathcal{N}_{\text{inst}}(t, k) \equiv \frac{z(t, k) \mathcal{H}(\nu(t), z(t, k))}{2k\epsilon(t)a^2(t)}, \quad (28)$$

where we define,

$$\mathcal{H}(\nu, z) \equiv \frac{\pi}{2} \left| H_\nu^{(1)}(z) \right|^2, \quad \nu(t) \equiv \frac{1}{2} + \frac{1}{1-\epsilon(t)}, \quad z(t, k) \equiv \frac{k}{[1-\epsilon(t)]H(t)a(t)}. \quad (29)$$

However, the choice (28) has the undesirable effect of complicating the late time limits. The physical quantities $M(t, k)$ and $\mathcal{N}(t, k)$ freeze in to constant values soon after first horizon crossing, but continued evolution in $\epsilon(t)$ prevents $M_0(t, k)$ and $\mathcal{N}_0(t, k)$ from approaching constants. Hence the residual exponents $h(n, k)$ and $g(n, k)$ must evolve so as to cancel this effect.

We can make the late time limits simpler by adopting a piecewise choice for the approximate solutions,

$$M_0(t, k) = \theta(t_k - t)M_{\text{inst}}(t, k) + \theta(t - t_k)\overline{M}_{\text{inst}}(t, k), \quad (30)$$

$$\mathcal{N}_0(t, k) = \theta(t_k - t)\mathcal{N}_{\text{inst}}(t, k) + \theta(t - t_k)\overline{\mathcal{N}}_{\text{inst}}(t, k). \quad (31)$$

By $\overline{M}_{\text{inst}}(t, k)$ and $\overline{\mathcal{N}}_{\text{inst}}(t, k)$ we mean the solutions which would pertain for the ersatz geometry,

$$\overline{a}(n) = a(n) = a_k e^{\Delta n}, \quad \overline{H}(n) = H_k e^{-\epsilon_k \Delta n}, \quad \overline{\epsilon}(n) = \epsilon_k. \quad (32)$$

Here and henceforth $\Delta n \equiv n - n_k$ stands for the number of e-foldings from horizon crossing. To be explicit about the over-lined quantities,

$$\overline{M}_{\text{inst}} \equiv \frac{\overline{z} \mathcal{H}(\nu_k, \overline{z})}{2k\overline{a}^2}, \quad \overline{\mathcal{N}}_{\text{inst}} \equiv \frac{\overline{z} \mathcal{H}(\nu_k, \overline{z})}{2k\epsilon_k \overline{a}^2}, \quad \overline{z} \equiv \frac{e^{(1-\epsilon_k)\Delta n}}{1-\epsilon_k}. \quad (33)$$

With the choice (30-31) the approximate solutions rapidly freeze in to constants,

$$\lim_{t \gg t_k} M_0(t, k) = \frac{H_k^2}{2k^3} \times C(\epsilon_k), \quad \lim_{t \gg t_k} \mathcal{N}_0(t, k) = \frac{H_k^2}{2\epsilon_k k^3} \times C(\epsilon_k). \quad (34)$$

This establishes the forms (3-4) for the power spectra and fixes the nonlocal correction exponents to,

$$\tau[\epsilon](k) = -\frac{1}{2} \lim_{t \gg t_k} g(t, k), \quad \sigma[\epsilon](k) = -\frac{1}{2} \lim_{t \gg t_k} h(t, k). \quad (35)$$

It remains to specialize the sources to (30-31). First note the simple relation between the scalar and tensor frequencies,

$$\Omega(n, k) = \theta(n_n - n)\omega(n, k) + \theta(n - n_k)\omega(n, k) \times \frac{\epsilon_k}{\epsilon(n)}. \quad (36)$$

This means the scalar source (24) consists of the tensor source (13) minus a handful of terms mostly involving $\epsilon(n)$,

$$S_g(n, k) = S_h(n, k) - 2\theta(n_k - n) \left[\left(\frac{\epsilon'}{\epsilon} \right)' + \frac{1}{2} \left(\frac{\epsilon'}{\epsilon} \right)^2 + (3 - \epsilon) \frac{\epsilon'}{\epsilon} \right] \\ + 2\delta(n - n_k) \frac{\epsilon'}{\epsilon} - 2\theta(n - n_k) \left[\left(3 - \epsilon + \frac{\omega'}{\omega} \right) \frac{\epsilon'}{\epsilon} + \omega^2 \left(\frac{\epsilon_k^2}{\epsilon^2} - 1 \right) \right]. \quad (37)$$

To obtain an explicit formula for the tensor source we first note that the tensor frequency is,

$$\omega(n, k) = \theta(n_k - n) \frac{2(1 - \epsilon)}{\mathcal{H}(\nu, z)} + \theta(n - n_k) \frac{2(1 - \epsilon_k)}{\mathcal{H}(\nu_k, \bar{z})} \times \frac{\bar{H}}{H}. \quad (38)$$

Hence the n derivative of its logarithm is,

$$\frac{\omega'}{\omega} = \theta(n_k - n) \left[-\frac{\epsilon'}{1 - \epsilon} - \frac{\mathcal{H}'}{\mathcal{H}} \right] + \theta(n - n_k) \left[\Delta\epsilon - \frac{\bar{\mathcal{H}}'}{\bar{\mathcal{H}}} \right], \quad (39)$$

where $\Delta\epsilon \equiv \epsilon(n) - \epsilon_k$ and $\bar{\mathcal{H}} \equiv \mathcal{H}(\nu_k, \bar{z})$. Before horizon crossing $\nu = \frac{1}{2} + \frac{1}{1 - \epsilon}$ is time dependent and $z = k/[(1 - \epsilon)Ha]$ so we have,

$$\nu' = \frac{\epsilon'}{(1 - \epsilon)^2}, \quad z' = -\left[1 - \epsilon - \frac{\epsilon'}{1 - \epsilon} \right] z \\ \implies -\frac{\mathcal{H}'}{\mathcal{H}} = -\frac{\epsilon'}{(1 - \epsilon)^2} \mathcal{A} + \left[1 - \epsilon - \frac{\epsilon'}{1 - \epsilon} \right] \mathcal{B}, \quad (40)$$

where \mathcal{A} and \mathcal{B} involve derivatives of $\mathcal{H}(\nu, z)$ with respect to ν and $\zeta = \ln(z)$,

$$\mathcal{A} \equiv \partial_\nu \ln \left[\mathcal{H}(\nu, e^\zeta) \right] \quad , \quad \mathcal{B} \equiv \partial_\zeta \ln \left[\mathcal{H}(\nu, e^\zeta) \right]. \quad (41)$$

The analogous result after horizon crossing is much simpler,

$$-\frac{\bar{\mathcal{H}}'}{\bar{\mathcal{H}}} = (1 - \epsilon_k) \bar{\mathcal{B}}, \quad (42)$$

where $\bar{\mathcal{B}}$ means \mathcal{B} with ν specialized to ν_k and e^ζ specialized to \bar{z} .

Taking the derivative of ω'/ω before horizon crossing,

$$\left(\frac{\omega'}{\omega} \right)' = -\frac{\epsilon''}{1 - \epsilon} - \frac{\epsilon'^2}{(1 - \epsilon)^2} - \left[\frac{\epsilon''}{(1 - \epsilon)^2} + \frac{2\epsilon'^2}{(1 - \epsilon)^3} \right] \mathcal{A} - \left[\epsilon' + \frac{\epsilon''}{1 - \epsilon} + \frac{\epsilon'^2}{(1 - \epsilon)^2} \right] \mathcal{B} \\ - \frac{\epsilon'^2}{(1 - \epsilon)^4} \mathcal{C} + \frac{2\epsilon'}{(1 - \epsilon)^2} \left[1 - \epsilon - \frac{\epsilon'}{1 - \epsilon} \right] \mathcal{D} - \left[1 - \epsilon - \frac{\epsilon'}{1 - \epsilon} \right] \mathcal{E}, \quad (43)$$

requires three second derivatives of $\ln[\mathcal{H}]$,

$$\mathcal{C} \equiv \partial_\nu^2 \ln[\mathcal{H}(\nu, e^\zeta)] \quad , \quad \mathcal{D} \equiv \partial_\zeta \partial_\nu \ln[\mathcal{H}(\nu, e^\zeta)] \quad , \quad \mathcal{E} \equiv \partial_\zeta^2 \ln[\mathcal{H}(\nu, e^\zeta)] \quad . \quad (44)$$

Bessel's equation and the Wronskian of $H_\nu^{(1)}(e^\zeta)$ imply,

$$2(1-\epsilon)^2 \mathcal{E} + (1-\epsilon)^2 \mathcal{B}^2 - (3-\epsilon)^2 + 4(1-\epsilon)^2 e^{2\zeta} - \left(\frac{2(1-\epsilon)}{\mathcal{H}} \right)^2 = 0 \quad . \quad (45)$$

Substituting relations (39), (40), (43) and (45) in the definition of the tensor source (13) gives,

$$\begin{aligned} t < t_k \quad \implies \quad S_{\text{before}} = & \frac{2\epsilon''}{1-\epsilon} \left[1 + \frac{\mathcal{A}}{1-\epsilon} + \mathcal{B} \right] + 2\epsilon' \left[1 - \frac{\mathcal{A}\mathcal{B}}{1-\epsilon} - \mathcal{B}^2 - \frac{2\mathcal{D}}{1-\epsilon} - 2\mathcal{E} \right] \\ & + \frac{2\epsilon'^2}{(1-\epsilon)^2} \left\{ -\frac{1}{2} + \frac{1}{2} \left[2 + \frac{\mathcal{A}}{1-\epsilon} + \mathcal{B} \right]^2 + \frac{\mathcal{A}}{1-\epsilon} + \frac{\mathcal{C}}{(1-\epsilon)^2} + \frac{2\mathcal{D}}{1-\epsilon} + \mathcal{E} \right\} \quad . \quad (46) \end{aligned}$$

The analogous result after horizon crossing is,

$$\begin{aligned} t > t_k \quad \implies \quad S_{\text{after}} = & 2\Delta\epsilon \left[3 - \epsilon_k + (1 - \epsilon_k) \overline{\mathcal{B}} \right] \\ & + 4 \left[\frac{k^2}{\overline{H}^2 a^2} - \left(\frac{1 - \epsilon_k}{\overline{\mathcal{H}}} \right)^2 \right] \left[\frac{\overline{H}^2}{\overline{H}^2} - 1 \right] \quad . \quad (47) \end{aligned}$$

There is also a jump at horizon crossing so that the complete result is,

$$S_h = \theta(n_k - n) S_{\text{before}} - \delta(n - n_k) \frac{2\epsilon'}{1-\epsilon} \left[1 + \frac{\mathcal{A}}{1-\epsilon} + \mathcal{B} \right] + \theta(n - n_k) S_{\text{after}} \quad . \quad (48)$$

4 Simple Analytic Approximations

The exact analytic results of the previous section are valid for all single-scalar models of inflation. However, they can be wonderfully simplified by exploiting the fact that *the first slow roll parameter is very small*. The 95% confidence bound on the tensor-to-scalar ratio of $r < 0.12$ [24, 25] implies $\epsilon < 0.0075$. This suggests a number of approximations. First, the local slow roll correction factor $C(\epsilon_k)$, defined in (5), may as well be set to unity. From Figure 2 we see that the bound of $\epsilon < 0.0075$ implies $1.0000 < C(\epsilon_k) < 0.9959$. This is not currently resolvable.

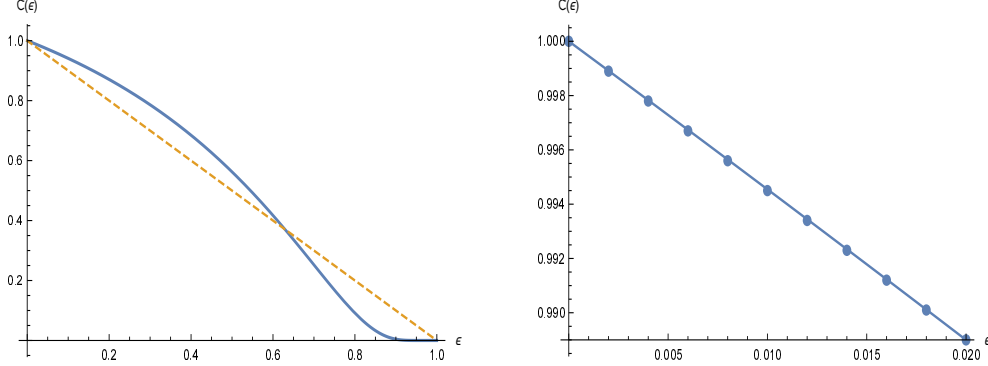


Figure 2: The left hand graph shows the local slow roll correction factor $C(\epsilon)$ (solid blue), which was defined in expression (5). Also shown is its global approximation of $1 - \epsilon$ (dashed yellow) over the full inflationary range of $0 \leq \epsilon < 1$. The right hand graph shows $C(\epsilon)$ (solid blue) versus the better approximation of $1 - 0.55\epsilon$ (large dots) relevant to the range $0 \leq \epsilon < 0.02$ favored by current data.

Another excellent approximation is taking $\epsilon = 0$ in the tensor and scalar Green's functions of expressions (14) and (25),

$$\begin{aligned} \lim_{\epsilon=0} G_h(n; m) &= \lim_{\epsilon=0} G_g(n; m) \equiv G_0(n; m) \\ &= \frac{\theta(n-m)}{2} \left[e^{\Delta m} + e^{3\Delta m} \right] \sin \left[-2 \left\{ e^{-\Delta \ell} - \arctan \left(e^{-\Delta \ell} \right) \right\} \Big|_m^n \right], \end{aligned} \quad (49)$$

where $\Delta m \equiv m - n_k$ and $\Delta \ell \equiv \ell - n_k$. Note that this expression is valid before and after horizon crossing. An important special case of (49) is when n becomes large, which gives the function $G(e^{\Delta m})$ we define as,

$$G(x) \equiv \frac{1}{2} \left(x + x^3 \right) \sin \left[\frac{2}{x} - 2 \arctan \left(\frac{1}{x} \right) \right]. \quad (50)$$

From the graph in Figure 3 we see that $G(e^{\Delta n})$ suppresses contributions more than a few e-foldings before horizon crossing.

We can also take $\epsilon = 0$ in \mathcal{H} and the derivatives of it in expressions (41) and (44). This leads to exact results for \mathcal{H} , \mathcal{B} and \mathcal{E} in terms of the parameter $x \equiv e^{\Delta n}$,

$$\lim_{\epsilon=0} \mathcal{H} \equiv \mathcal{H}_0(x) = x + x^3, \quad (51)$$

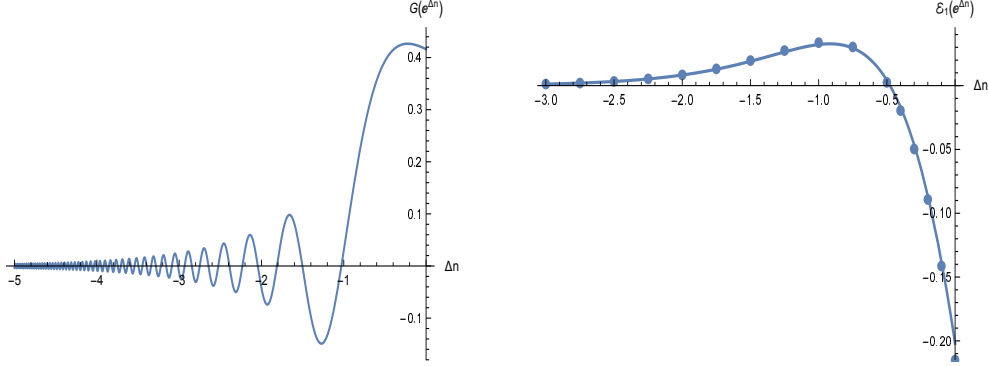


Figure 3: The left hand graph shows the $\epsilon = 0$ Green's function $G(e^{\Delta n})$ given in expression (50). The right hand graph shows the coefficient of $\epsilon''(n)$ in the small ϵ form (58) for $S_h(n, k)$. This function $\mathcal{E}_1(x)$ is defined by expressions (52), (54) and (59). The solid blue curve gives the exact numerical result while the large dots give the approximation resulting from the series expansion on the right hand side of expression (54).

$$\lim_{\epsilon=0} \mathcal{B} \equiv \mathcal{B}_0(x) = \frac{-1-3x^2}{1+x^2}, \quad (52)$$

$$\lim_{\epsilon=0} \mathcal{E} \equiv \mathcal{E}_0(x) = \frac{4x^2}{(1+x^2)^2}. \quad (53)$$

The three derivatives with respect to ν do not lead to simple expressions even for $\epsilon \rightarrow 0$, but they can be well approximated over the range we require by short series expansions in powers of x^2 ,

$$\lim_{\epsilon=0} \mathcal{A} \equiv \mathcal{A}_0(x) \simeq \frac{1.5x^2 + 1.8x^4 - 1.5x^6 + .63x^8}{1+x^2}, \quad (54)$$

$$\lim_{\epsilon=0} \mathcal{C} \equiv \mathcal{C}_0(x) \simeq \frac{x^2 + 6.1x^4 - 3.7x^6 + 1.6x^8}{(1+x^2)^2}, \quad (55)$$

$$\lim_{\epsilon=0} \mathcal{D} \equiv \mathcal{D}_0(x) \simeq \frac{-3x^2 - 6.8x^4 + 5.5x^6 - 2.6x^8}{(1+x^2)^2}. \quad (56)$$

We can express the ratio of \overline{H}/H in terms of the deviation $\Delta\epsilon(n) \equiv \epsilon(n) - \epsilon_k$,

$$\frac{\overline{H}^2}{H^2} - 1 = \exp \left[2 \int_{n_k}^n dm \Delta\epsilon(m) \right] - 1 \simeq 2 \int_{n_k}^n dm \Delta\epsilon(m). \quad (57)$$

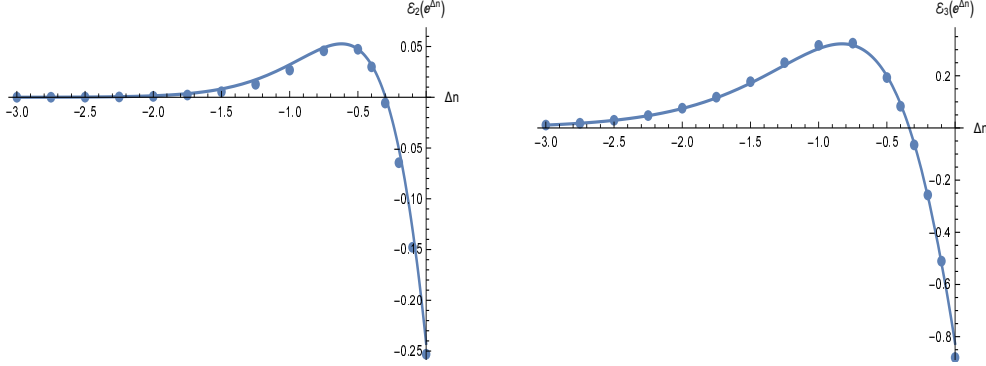


Figure 4: The coefficients of $[\varepsilon'(n)]^2$ (left) and $\varepsilon'(n)$ (right) in the small ϵ form (58) for $S_h(n, k)$. In each case the solid blue curve gives the exact numerical result, while the large dots give the result of using the series approximations on the far right of (54-56) in expressions (60) and (61).

All of this gives an approximation for the tensor source (48),

$$S_h(n, k) \simeq -2\theta(-\Delta n) \left[\epsilon'' \mathcal{E}_1(e^{\Delta n}) + \epsilon'^2 \mathcal{E}_2(e^{\Delta n}) + \epsilon' \mathcal{E}_3(e^{\Delta n}) \right] + 2\delta(\Delta n) \epsilon' \mathcal{E}_1(1) \\ + 2\theta(\Delta n) \left\{ \Delta \epsilon(n) + \left(\frac{4 + 2e^{2\Delta n}}{1 + e^{2\Delta n}} \right) \int_{n_k}^n dm \Delta \epsilon(m) \right\} \frac{2}{1 + e^{2\Delta n}}, \quad (58)$$

where the three coefficient functions are,

$$\mathcal{E}_1(x) = -1 - \mathcal{A}_0(x) - \mathcal{B}_0(x), \quad (59)$$

$$\mathcal{E}_2(x) = \frac{1}{2} - \mathcal{A}_0(x) - \mathcal{C}_0(x) - 2\mathcal{D}_0(x) - \mathcal{E}_0(x) - \frac{1}{2} \left[2 + \mathcal{A}_0(x) + \mathcal{B}_0(x) \right]^2, \quad (60)$$

$$\mathcal{E}_3(x) = -1 + \mathcal{A}_0(x) \mathcal{B}_0(x) + \mathcal{B}_0^2(x) + 2\mathcal{D}_0(x) + 2\mathcal{E}_0(x). \quad (61)$$

Figures 3 and 4 show the various coefficient functions.

The smallness of ϵ means that the factors of $1/\epsilon$ which occur in the scalar source (37) are hugely important. By comparison we can ignore the $S_h(n, k)$ terms and simply write,

$$S_g(n, k) \simeq -2\theta(-\Delta n) \left[\left(\frac{\epsilon'}{\epsilon} \right)' + \frac{1}{2} \left(\frac{\epsilon'}{\epsilon} \right)^2 + 3 \frac{\epsilon'}{\epsilon} \right] + 2\delta(\Delta n) \frac{\epsilon'}{\epsilon} - 2\theta(\Delta n) \frac{\epsilon'}{\epsilon} \frac{2}{1 + e^{2\Delta n}}. \quad (62)$$

Because $\epsilon < 0.0075$ we expect S_g to be more than 100 times as strong as S_h .

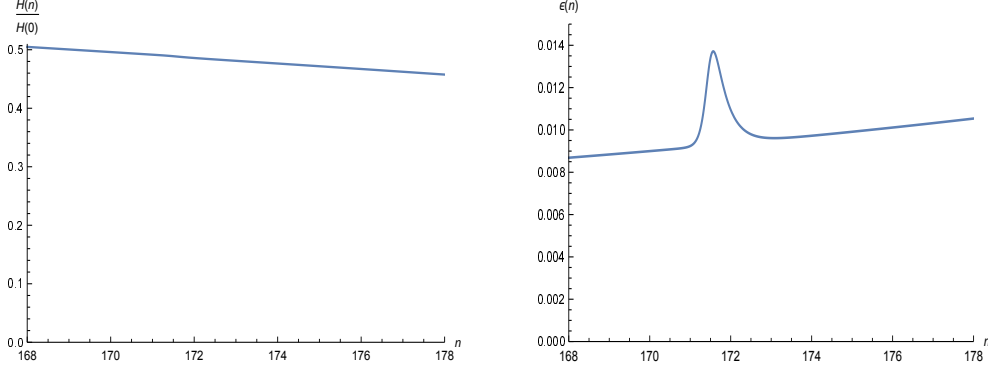


Figure 5: The left hand figure shows the Hubble parameter and the right shows the first slow roll parameter for a model with features. This model which was proposed [28, 29] to explain the observed features in the scalar power spectrum at $\ell \approx 22$ and $\ell \approx 40$ which are visible in the data reported from both WMAP [27, 30] and PLANCK [31, 32]. Note that the feature has little impact on $H(n)$ but it does lead to a distinct bump in $\epsilon(n)$.

The approximations (49), (58) and (62) are valid so long as ϵ is small. If we additionally ignore nonlinear terms in the equations for $h(n, k)$ and $g(n, k)$, the correction exponents of expressions (3-4) become,

$$\begin{aligned} \tau[\epsilon](k) \simeq & \int_0^{n_k} dn \left[\epsilon''(n) \mathcal{E}_1(e^{\Delta n}) + [\epsilon'(n)]^2 \mathcal{E}_2(e^{\Delta n}) + \epsilon'(n) \mathcal{E}_3(e^{\Delta n}) \right] G(e^{\Delta n}) \\ & - \epsilon'(n_k) \mathcal{E}_1(1) G(1) - \int_{n_k}^{\infty} dn \left\{ \Delta \epsilon(n) + \left(\frac{4 + 2e^{2\Delta n}}{1 + e^{2\Delta n}} \right) \int_{n_k}^n dm \Delta \epsilon(m) \right\} \frac{2G(e^{\Delta n})}{1 + e^{2\Delta n}}, \quad (63) \end{aligned}$$

$$\begin{aligned} \sigma[\epsilon](k) \simeq & \int_0^{n_k} dn \left[\partial_n^2 \ln[\epsilon(n)] + \frac{1}{2} \left(\partial_n \ln[\epsilon(n)] \right)^2 + 3 \partial_n \ln[\epsilon(n)] \right] G(e^{\Delta n}) \\ & - \partial_{n_k} \ln[\epsilon(n_k)] G(1) + \int_{n_k}^{\infty} dn \partial_n \ln[\epsilon(n)] \frac{2G(e^{\Delta n})}{1 + e^{2\Delta n}}. \quad (64) \end{aligned}$$

Recall that $\Delta n \equiv n - n_k$, $\Delta \epsilon(n) \equiv \epsilon(n) - \epsilon_k$, the Green's function $G(e^{\Delta n})$ was defined in (50), and the coefficient functions $\mathcal{E}_1(e^{\Delta n})$, $\mathcal{E}_2(e^{\Delta n})$ and $\mathcal{E}_3(e^{\Delta n})$ were given in expressions (59-61).

How large $\tau[\epsilon](k)$ and $\sigma[\epsilon](k)$ are depends on what the inflationary model predicts for derivatives of $\epsilon(n)$. For example, the slow roll approximation of

monomial inflation gives,

$$V(\varphi) = A\varphi^\alpha \quad \Longrightarrow \quad \epsilon(n) \simeq \frac{\epsilon_i}{1 - \frac{4}{\alpha}\epsilon_i n} . \quad (65)$$

For these models the various tensor and scalar contributions are small,

$$V(\varphi) = A\varphi^\alpha \quad \Longrightarrow \quad \epsilon'' \simeq \frac{32}{\alpha^2} \epsilon^3 , \quad \epsilon'^2 \simeq \frac{16}{\alpha^2} \epsilon^4 , \quad \epsilon' \simeq \frac{4}{\alpha} \epsilon^2 , \quad (66)$$

$$\Longrightarrow \quad \left(\frac{\epsilon'}{\epsilon}\right)' \simeq \frac{16}{\alpha^2} \epsilon^2 , \quad \left(\frac{\epsilon'}{\epsilon}\right)^2 \simeq \frac{16}{\alpha^2} \epsilon^2 , \quad \frac{\epsilon'}{\epsilon} \simeq \frac{4}{\alpha} \epsilon . \quad (67)$$

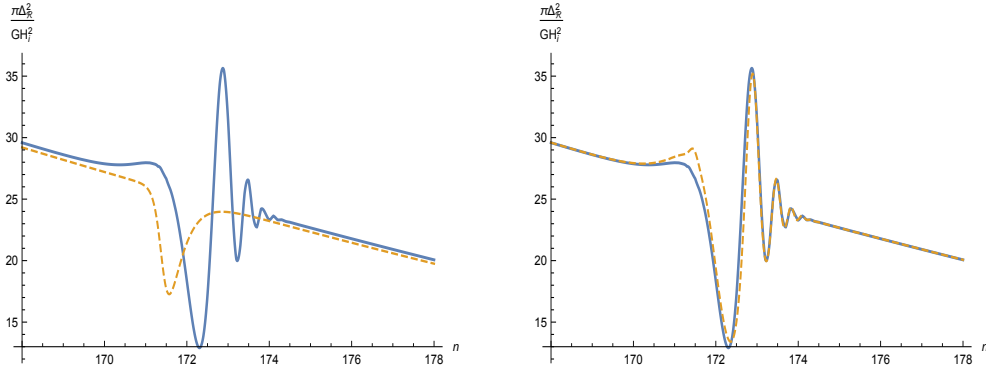


Figure 6: These graphs show the scalar power spectrum for the model of Figure 5. The left hand figure compares the exact result (solid blue) with the local slow roll approximation $\Delta_{\mathcal{R}}^2(k) \approx GH_k^2/\pi\epsilon_k \times C(\epsilon_k)$ (yellow dashed). The right hand figure compares the exact result (solid blue) with the much better approximation (yellow dashed) obtained from multiplying by $\exp[\sigma[\epsilon](k)]$, using our analytic approximation (64) for $\sigma[\epsilon](k)$.

The data disfavors monomial inflation [24, 25, 26], but $\tau[\epsilon](k)$ and $\sigma[\epsilon](k)$ will be small for any model which has only slow evolution of $\epsilon(n)$. Much larger effects occur for models with “features”, which are transient fluctuations above or below the usual smooth fits [27]. Features imply short-lived changes in $\epsilon(n)$, which do not have much effect on $H(n)$ but can lead to large values of $\epsilon'(n)$ and $\epsilon''(n)$. Figure 5 shows $H(n)$ and $\epsilon(n)$ for a model that was proposed [28, 29] to explain a deficit at $\ell \approx 22$, and an excess at $\ell \approx 40$, in the data reported by both WMAP [27, 30] and PLANCK [31, 32]. In the range $171 < n < 172.5$ the scalar experiences a step in its potential which has little effect on $H(n)$ but leads to a noticeable bump in $\epsilon(n)$.

Figure 6 shows the scalar power spectrum for the model of Figure 5. The left hand graph compares the exact result to the local slow roll approximation, without including the nonlocal corrections from $\sigma[\epsilon](k)$. Not even the main feature is correct, and the secondary oscillations are completely absent. There is also a small systematic offset before and after the features. The right hand graph shows the effect of adding $\sigma[\epsilon](k)$ with our approximation (64). The agreement is almost perfect, with the small remaining deviations attributable to nonlinear effects. The small offset of the left hand graph (before and after the features) is due to the local slow roll approximation missing the steady growth which $\epsilon(n)$ needs to reach the threshold of $\epsilon = 1$ at which inflation ends. We conclude:

1. The nonlocal correction $\sigma[\epsilon](k)$ fixes the systematic under-prediction of the local slow roll approximation when $\epsilon(n)$ is growing steadily;
2. The nonlocal correction $\sigma[\epsilon](k)$ makes large and essential contributions when features are present; and
3. The nonlocal correction $\sigma[\epsilon](k)$ is well approximated by (64).

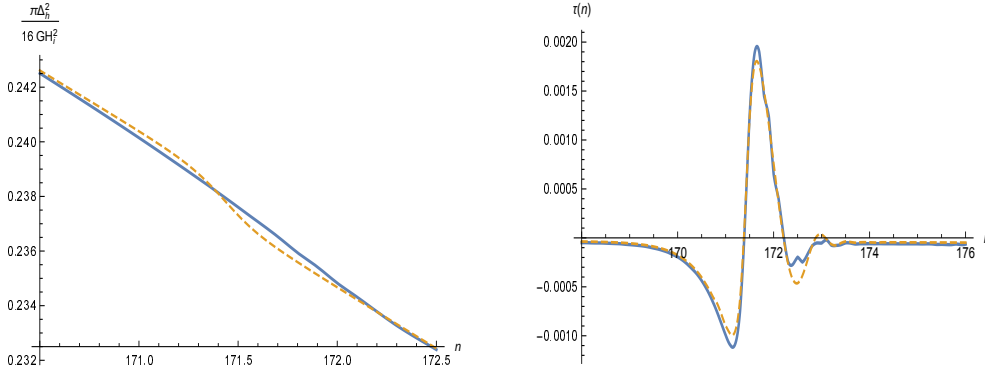


Figure 7: These graphs show the tensor power spectrum for the model of Figure 5. The left hand figure compares the exact result (solid blue) with the local slow roll approximation $\Delta_h^2(k) \approx \frac{16}{\pi} G H_k^2 C(\epsilon_k)$ (yellow dashed). The solid blue line on the right hand graph shows the logarithm of the ratio of $\Delta_h^2(k)$ to its local slow roll approximation. The yellow dashed line gives the nonlocal corrections of expression (63).

Figure 7 shows the tensor power spectrum for the model of Figure 5. The left hand graph compares the exact result with the local slow roll approx-

imation. The prominent features of the scalar power spectrum which can be seen in Figure 6 are several hundred times smaller, inverted and phase shifted, but they can just be made out. The right hand graph compares our approximation (63) for $\tau[\epsilon](k)$ with the exact result. The agreement is again almost perfect, with the small deviations actually attributable to numerical roughness in the interpolation of the exact computation, rather than to any problem with our approximation (63). Correlating tensor features with their much stronger scalar counterparts might be possible in the far future and would represent an impressive confirmation of single-scalar inflation [21].

5 Reconstructing the Geometry

We have so far considered the problem of using the inflationary geometry to predict the power spectra. Here we wish to consider the inverse problem of using $\Delta_{\mathcal{R}}^2(k)$ and $\Delta_h^2(k)$ to reconstruct $H(n)$ and $\epsilon(n)$. (The scalar and its potential can be derived from $H(n)$ and $\epsilon(n)$ by the formulae given in footnote 1.) It is well to begin by setting down a few general principles:

1. Although $\Delta_{\mathcal{R}}^2(k)$ is measured to 3-digit accuracy, the tensor power spectrum has yet to be resolved. When $\Delta_h^2(k)$ is finally detected it will take a number of years before much precision is attained. Therefore, reconstruction should be based on $\Delta_{\mathcal{R}}^2(k)$, with $\Delta_h^2(k)$ used only to fix the integration constant which gives the scale of inflation.
2. The first slow roll parameter is so small that there is no point in using the exact expression (4) for $\Delta_{\mathcal{R}}^2(k)$. Figure 2 shows that we can ignore the local slow roll correction factor $C(\epsilon_k)$. Although the nonlocal correction exponent $\sigma[\epsilon](k)$ must be included, Figure 6 shows that the approximation (64) is almost perfect.
3. The fact that $\epsilon(n)$ is small and smooth, with small transients, motivates a hierarchy between H , ϵ and ϵ'/ϵ based on calculus,

$$H(n) = H_i \exp \left[- \int_0^n dm \epsilon(m) \right] , \quad \epsilon(n) = \epsilon_i \exp \left[\int_0^n dm \frac{\epsilon'(m)}{\epsilon(m)} \right] . \quad (68)$$

Hence $H(n)$ is insensitive to small errors in $\epsilon(n)$, and $\epsilon(n)$ is insensitive to small errors in $\partial_n \ln[\epsilon(n)]$.

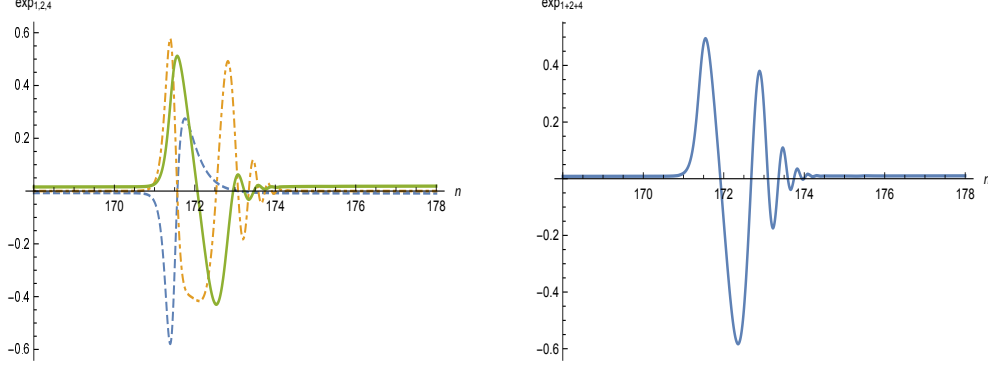


Figure 8: Numerical values of exponents 1, 2 and 4 for the model of Figure 5. The left hand graph gives separate results for expression (71) in dashed blue, expression (72) in dot-dashed yellow, and expression (74) in solid green. The right hand graph shows the sum of all three exponents.

We begin by converting from wave number k to n_k , the number of e-foldings since the beginning of inflation that k experienced first horizon crossing. It is also desirable to factor out the scale of inflation $H_i \equiv H(0)$,

$$h(n) \equiv \frac{H(n)}{H_i} \quad , \quad \delta(n_k) \equiv \frac{\pi \Delta_{\mathcal{R}}^2(k)}{G H_i^2} . \quad (69)$$

(H_i is the single number which would come from the tensor power spectrum.) Based on the three principles we base reconstruction on the formula,

$$\delta(n) \simeq \frac{h^2(n)}{\epsilon(n)} \times \exp \left[\sum_{i=1}^5 \exp_i(n) \right] , \quad (70)$$

where the five exponents follow from our approximation (64) for $\sigma[\epsilon](k)$,

$$\exp_1(n) = -\partial_n \ln[\epsilon(n)] \times G(1) , \quad (71)$$

$$\exp_2(n) = \int_0^n dm \partial_m^2 \ln[\epsilon(m)] \times G(e^{m-n}) , \quad (72)$$

$$\exp_3(n) = \frac{1}{2} \int_0^n dm \left[\partial_m \ln[\epsilon(m)] \right]^2 \times G(e^{m-n}) , \quad (73)$$

$$\exp_4(n) = 3 \int_0^n dm \partial_m \ln[\epsilon(m)] \times G(e^{m-n}) , \quad (74)$$

$$\exp_5(n) = 2 \int_n^\infty dm \partial_m \ln[\epsilon(m)] \times \frac{G(e^{m-n})}{1+e^{2(m-n)}} . \quad (75)$$

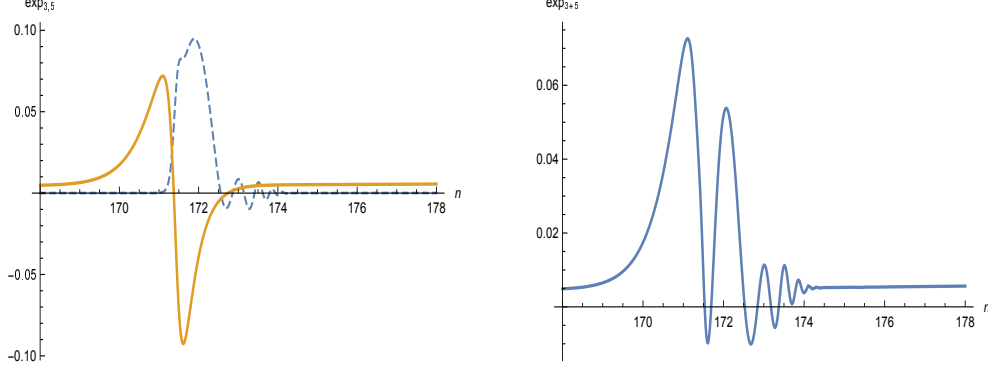


Figure 9: Numerical values of $\exp_3(n)$ and $\exp_5(n)$ for the model of Figure 5. The left hand graph gives separate results for expression (73) in dashed blue, and expression (75) in solid yellow. Note that $\exp_5(n)$ is responsible for correcting the small, systematic under-prediction of the slow roll approximation before and after the feature. The right hand graph shows the sum.

To just reconstruct the Hubble parameter there is no need to include the correction exponents (71-75). Using only the leading slow roll terms gives,

$$\delta(n) \simeq \frac{h^2(n)}{\epsilon(n)} \implies h^2(n) \simeq \frac{1}{1 + \int_0^n \frac{2dm}{\delta(m)}}. \quad (76)$$

Even for the power spectrum of Figure 6 the reconstruction of $h(n)$ given by expression (76) is barely distinguishable from the left hand graph of figure 5.

Not all the exponents (71-75) are equally important. Figures 8 and 9 show that the set of $\exp_1(n)$, $\exp_2(n)$ and $\exp_4(n)$ are about ten times larger than $\exp_3(n)$ and $\exp_5(n)$ for the model of Figure 5. That reconstructing features indeed requires the three large exponents is apparent from Figure 10. Taking the logarithm of (70) and moving the three large exponents to the left gives,

$$\begin{aligned} \left[1 + G(1)\partial_n\right] \ln[\epsilon(n)] - \int_0^n dm \left[\partial_m^2 + 3\partial_m\right] \ln[\epsilon(m)] \times G(e^{m-n}) \\ \simeq -\ln[\delta(n)] + 2\ln[h(n)] + \exp_3(n) + \exp_5(n). \end{aligned} \quad (77)$$

This becomes a linear, nonlocal equation for $\ln[\epsilon(n)]$ if we drop $\exp_3(n)$ and $\exp_5(n)$ and use expression (76) for the Hubble parameter,

$$\begin{aligned} \left[1 + G(1)\partial_n\right] \ln[\epsilon(n)] - \int_0^n dm \left[\partial_m^2 + 3\partial_m\right] \ln[\epsilon(m)] \times G(e^{m-n}) \\ \simeq -\ln[\delta(n)] - \ln\left[1 + \int_0^n \frac{2dm}{\delta(m)}\right]. \end{aligned} \quad (78)$$

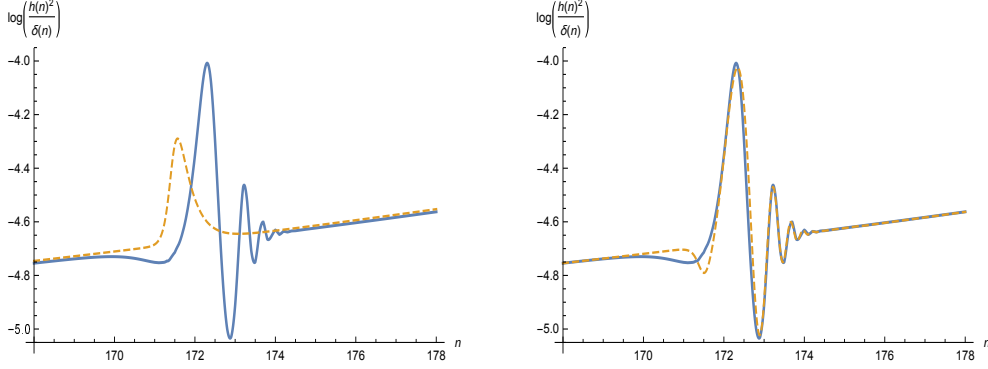


Figure 10: Various choices for the left hand side of the first pass reconstruction equation for the model of Figure 5. The left hand graph shows the first pass source $-\ln[\delta(n)] + 2\ln[h(n)]$ in solid blue with $\ln[\epsilon(n)]$ overlaid in dashed yellow. The poor agreement between the two curves is why using just $\ln[\epsilon(n)]$ as the left hand side of the first pass reconstruction fails to converge when features are present. The right hand graph shows the much better agreement between the same source (solid blue) and $\ln[\epsilon(n)] - \exp_1(n) - \exp_2(n) - \exp_4(n)$ (dashed yellow).

The linearity of equation (78) means that it can be solved by a Green's function, in spite of being nonlocal. The required Green's function becomes a symmetric function of its arguments if we note from Figure 3 and expression (50) that $G(e^{n-n_k})$ is essentially zero more than about $N \sim 4$ e-foldings before horizon crossing. The Green's function equation is,

$$\left[1 + G(1)\partial_n\right]\mathcal{G}(n) - \int_{-N}^n dm (\partial_m^2 + 3\partial_m)\mathcal{G}(m) \times G(e^{m-n}) = \delta(n) . \quad (79)$$

We can solve (78) by integrating against the source on the right hand side,

$$\ln[\epsilon(n)] = \int_0^\infty dm \mathcal{G}(n-m) \times \text{Source}(m) . \quad (80)$$

This might be regarded as the first pass of an iterative solution to (77). After the first pass solution of (78) one would use the resulting $\ln[\epsilon(n)]$ to construct $h(n)$ and to evaluate $\exp_3(n)$ and $\exp_5(n)$ on the right hand side of (77). Then the same Green's function solution (80) could be used with this more accurate source to find a more accurate $\ln[\epsilon(n)]$, which would lead to a more accurate source, and so on.

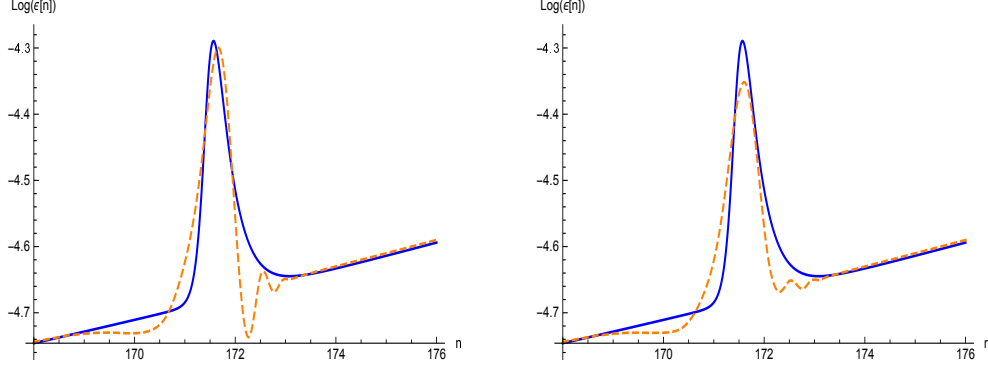


Figure 11: These graphs show numerical reconstructions of $\ln[\epsilon(n)]$ for the power spectrum of Figure 6. The solid blue line of the left hand graph shows the exact result while the yellow dashed line gives the result of integrating $\mathcal{G}_0(n-m)$ — using the first six terms of the sum over ℓ in expression (83) — against the first pass source on the right hand side of (78). The right hand graph shows the result of adding the first order improvement $\mathcal{G}_1(n-m)$ — computed using the first four terms of the sum over m in expression (92).

We are not able to solve (79) exactly owing to the factor of $G(e^{m-n})$ inside the integral. Consideration of Figure 3 suggests that this troublesome factor might be approximated as a square wave of width $\Delta = 0.8$,

$$G(e^{m-n}) \approx G(1)\theta(n-m-\Delta) . \quad (81)$$

Making the approximation (81) leads to a still-nonlocal equation,

$$(\partial_n + 3)\mathcal{G}_0(n-\Delta) - \alpha\mathcal{G}_0(n) = \frac{\delta(n)}{G(1)} \quad , \quad \alpha \equiv 3 - \frac{1}{G(1)} . \quad (82)$$

The “retarded” solution to (82) which avoids exponentially growing terms is,

$$\mathcal{G}_0(n) = \frac{e^{3(n+\Delta)}}{G(1)} \sum_{\ell=0}^{\infty} \frac{1}{\ell!} \left[\alpha e^{-3\Delta} \left(n + (\ell+1)\Delta \right) \right]^\ell \theta\left(n + (\ell+1)\Delta \right) . \quad (83)$$

Figure 11 shows the result of using just $\mathcal{G}_0(n)$ to reconstruct $\ln[\epsilon(n)]$ with the source taken as the right hand side of (78).

Further improvement requires a better approximation for the Green’s function $\mathcal{G}(n)$. It is instructive to take the Laplace transform, restoring the

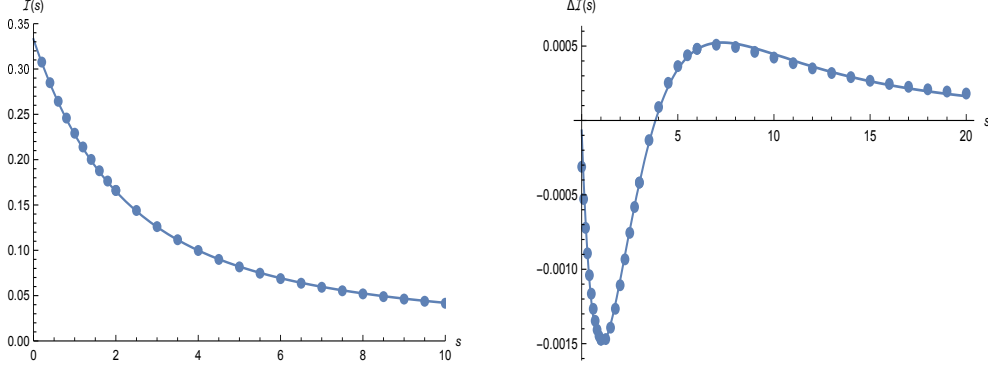


Figure 12: The solid blue line of the left hand graph shows a numerical evaluation of the integral $\mathcal{I}(s)$ of expression (86). The 0th order approximation $\mathcal{I}_0(s)$ of expression (87) is overlaid in large dots. The solid blue line of the right hand graph shows the deviation $\Delta\mathcal{I}(s) \equiv \mathcal{I}(s) - \mathcal{I}_0(s)$. Our fit $\mathcal{I}_1(s)$ of expression (88) is overlaid in large dots.

second argument of the Green's function,

$$\widehat{\mathcal{G}}(s; m) \equiv \int_0^\infty dn e^{-sn} \mathcal{G}(n-m) . \quad (84)$$

The Laplace transform of the Green's function equation (79) is,

$$\left[1 + G(1)s - (s+3)s \times \mathcal{I}(s)\right] \widehat{\mathcal{G}}(s; m) = e^{-ms} , \quad (85)$$

where we define,

$$\mathcal{I}(s) \equiv \int_0^\infty d\ell e^{-s\ell} \times G(e^{-\ell}) . \quad (86)$$

The problem of approximating $\mathcal{G}(n-m)$ is therefore related to the one of approximating (86), and of recognizing the resulting inverse Laplace transform of $\widehat{\mathcal{G}}(s; m)$. Making the approximation (81) in (86) gives,

$$\mathcal{I}_0(s) = \frac{G(1)}{s} \left[1 - e^{-0.8s}\right] . \quad (87)$$

Figure 12 reveals that this is indeed a good approximation. Figure 12 also shows that the small residual is well fit by the function,

$$\mathcal{I}_1(s) = \frac{0.154}{(s + 8.97)^2} \sin \left[1.76 \left(1 - e^{-0.262(s-3.78)} \right) \right] . \quad (88)$$

To obtain the first correction to $\mathcal{G}_0(n-m)$ we begin by expanding $\widehat{\mathcal{G}}(s; m)$ in powers of $\mathcal{I}_1(s)$,

$$\widehat{\mathcal{G}}(s; m) \simeq \frac{e^{-ms}}{G(1)[(s+3)e^{-\Delta s} - \alpha] - s(s+3)\mathcal{I}_1(s)} , \quad (89)$$

$$= \frac{e^{-ms}}{G(1)[(s+3)e^{-\Delta s} - \alpha]} + \frac{s(s+3)\mathcal{I}_1(s)e^{-ms}}{G^2(1)[(s+3)e^{-\Delta s} - \alpha]^2} + \dots , \quad (90)$$

$$\equiv \widehat{\mathcal{G}}_0(s; m) + \widehat{\mathcal{G}}_1(s; m) + \dots \quad (91)$$

We can recognize the inverse Laplace transform by expanding $\mathcal{I}_1(s)$,

$$\begin{aligned} \frac{a}{(s+e)^2} \sin \left[b - be^{-c(s+d)} \right] &= \frac{a}{(s+e)^2} \left\{ \sin(b) \sum_{m=0}^{\infty} \frac{(-1)^m}{(2m)!} \left[be^{-c(s+d)} \right]^{2m} \right. \\ &\quad \left. - \cos(b) \sum_{m=0}^{\infty} \frac{(-1)^m}{(2m+1)!} \left[be^{-c(s+d)} \right]^{2m+1} \right\} . \end{aligned} \quad (92)$$

Figure 11 shows the effect of using $\mathcal{G}_0(n-m) + \mathcal{G}_1(n-m)$ to solve equation (78) approximately for $\ln[\epsilon(n)]$.

Figure 11 shows that additional improvements are needed before our technique gives good results for $\partial_n \ln[\epsilon(n)]$ when features are present. However, our results for $\epsilon(n)$ are already reasonable, and those for $h(n)$ are staggeringly accurate. For the model of Figure 5 the largest percentage error on in reconstructing $\epsilon(n)$ is 2.2%, and the percentage error for $h(n)$ never exceeds 0.04%. This seems considerably better than the General Slow Roll Approximation [33], or techniques based on local expressions [34]. A recent proposal based on inverse-scattering [35] reports percentage errors of $h(n)$ of as much as 2% for flat potentials, and up to 9% when features are present.

It is significant that our Green's function $\mathcal{G}(n-m)$ depends only on the difference of its arguments, and we just need it over a range of about ten e-foldings. Further, its Laplace transform is defined by relations (85-86). Figure 12 shows that there is only a single, simple pole on the real axis, somewhat below $s = 3$. If nothing else worked we could therefore evaluate $\mathcal{I}(s_0 + i\omega)$ numerically for some $s_0 > 3$ and then numerically compute the inverse Laplace transform,

$$\mathcal{G}(n-m) = \frac{1}{2\pi i} \int_{-\infty}^{\infty} d\omega e^{(s_0+i\omega)n} \widehat{\mathcal{G}}(s_0+i\omega; m) . \quad (93)$$

No matter how time-consuming the computation proved, it would only need to be done once.

6 Epilogue

As its title suggests, this paper gives final expression to our formalism for finding the tree order power spectra by evolving the norm-squared mode functions [20]. Considered purely as a numerical technique this is more efficient than evolving the mode functions because it avoids keeping track of the rapidly fluctuating phase, and because it converges about twice as fast. Nor is anything lost because the phase can be recovered through expressions (10) and (20). Our formalism applies not only to single-scalar inflation but also to any conformally related model, such as $f(R)$ inflation [22], whose power spectra are numerically identical.

Section 2 reviews our formalism, and explains how to factor out arbitrary approximate solutions (12) and (22). Section 3 then specializes to what we believe are the best choices (30-31) for these approximate solutions. Our results (3-4) for the power spectra are exact at this stage, with the nonlocal correction exponents $\tau[\epsilon](k)$ and $\sigma[\epsilon](k)$ given by (35).

Section 5 makes the approximation that $\epsilon(n)$ is small, and that nonlinear effects can be dropped in the equations (12) and (22) for the residuals. This results in wonderfully simple, analytic approximations (63-64) for how the nonlocal correction exponents depend upon $\epsilon(n)$. Figures 6 and 7 exhibit the accuracy of these formulae, even for the model of Figure 5 which has prominent features. Figure 6 also demonstrates that the local slow roll approximation — $\Delta_{\mathcal{R}}^2(k) \approx \frac{GH_k^2}{\pi\epsilon_k} \times C(\epsilon_k)$ — breaks down badly when features are present, and that it systematically underestimates $\Delta_{\mathcal{R}}^2(k)$ even for models without features. The unmistakable conclusions are:

1. That quantitative accuracy requires the nonlocal correction exponents $\tau[\epsilon](k)$ and $\sigma[\epsilon](k)$; and
2. That our approximations (63-64) are valid for any model which is consistent with the bounds on r and on the limits of possible features.

Section 5 explains how our approximation (64) can be used to reconstruct the geometry from the power spectra. (The scalar and its potential can be recovered from the formulae of footnote 1.) Further improvements are needed for accurate reconstructions for derivatives of the first slow roll parameter, but the undifferentiated parameter is accurate to $\pm 2.2\%$ and our errors for the Hubble parameter never exceed 0.04%. This seems much better than other techniques [33, 34, 35].

Our formalism has many applications because it gives explicit, analytic and accurate approximations for how the power spectra depend functionally on the geometry of inflation. For example, our expressions (3-4) imply an exact relation for the tensor-to-scalar ratio,

$$r(k) = 16\epsilon_k \exp\left[-\sigma[\epsilon](k) + \tau[\epsilon](k)\right], \quad (94)$$

with no local, slow roll corrections. It should be an excellent approximation to drop $\tau[\epsilon](k)$ and employ the analytic approximation (64) for $\sigma[\epsilon](k)$.

We have already mentioned the necessity of including the nonlocal correction exponent $\sigma[\epsilon](k)$ to correctly describe features. Our analytic approximation (64) facilitates precision studies, limited by the accuracy of the data rather than by the cumbersome connection to theory. For example, the model of Figure 5 was proposed [28, 29] to account for the deficit in the scalar power spectrum at $\ell \approx 22$, and the excess at $\ell \approx 40$, which are visible in the data reported from both WMAP [27, 30] and PLANCK [31, 32]. From Figure 6 we see that the resulting power spectrum indeed has a deficit at $n \approx 172.3$, followed by an excess at $n \approx 172.8$. However, there are weaker features at $n \approx 173.2$ and $n \approx 173.5$. Do the data show any evidence for these weaker features? If not, to what degree does their absence rule out the model of Figure 5? And what sort of model do the data actually support?

A particularly exciting application of our formalism is to exploit the control it gives over how the mode functions depend upon $\epsilon(n)$ to design a new statistic to cross-correlate features in the power spectrum with non-Gaussianity. This has already been proposed in the context of models with variable speed of sound [36, 37] but it can now be done with precision for simple scalar potential models. Of course the idea is that non-Gaussianity measures self-interaction, which is what a step in the potential provides. There may be an observable effect which is not resolvable by generic statistics but could be detected by a precision search.

Another application concerns the far future, after the tensor power spectrum has been well resolved. Our analytic approximations (63-64) quantify how the same derivatives of the first slow roll parameter lead to deviations from the local slow roll predictions for the tensor and scalar power spectra. Figure 6 shows that these deviations are strongly present in $\Delta_{\mathcal{R}}^2(k)$ for models with features. The associated tensor features are much weaker, but they can just be made out in Figure 7. Demonstrating this correlation in the data would represent an impressive check on single-scalar inflation.

In the even farther future it may be possible to resolve one loop corrections [23]. Comparing these with theory obviously requires a precision determination of the tree order effect, which is of course possible once the model of inflation has been fixed. However, one also needs to be able to extract the potentially large factors of $1/\epsilon(n)$ from the ζ propagator, and our formalism is ideal for that.

Acknowledgements

This work was partially supported by the European Union’s Seventh Framework Programme (FP7-REGPOT-2012-2013-1) under grant agreement number 316165; by the European Union’s Horizon 2020 Programme under grant agreement 669288-SM-GRAV-ERC-2014-ADG; by NSF grant PHY-1506513; and by the UF’s Institute for Fundamental Theory.

References

- [1] A. A. Starobinsky, JETP Lett. **30**, 682 (1979) [Pisma Zh. Eksp. Teor. Fiz. **30**, 719 (1979)].
- [2] V. F. Mukhanov and G. V. Chibisov, JETP Lett. **33**, 532 (1981) [Pisma Zh. Eksp. Teor. Fiz. **33**, 549 (1981)].
- [3] R. P. Woodard, Rept. Prog. Phys. **72**, 126002 (2009) doi:10.1088/0034-4885/72/12/126002 [arXiv:0907.4238 [gr-qc]].
- [4] A. Ashoorioon, P. S. Bhupal Dev and A. Mazumdar, Mod. Phys. Lett. A **29**, no. 30, 1450163 (2014) doi:10.1142/S0217732314501636 [arXiv:1211.4678 [hep-th]].
- [5] L. M. Krauss and F. Wilczek, Phys. Rev. D **89**, no. 4, 047501 (2014) doi:10.1103/PhysRevD.89.047501 [arXiv:1309.5343 [hep-th]].
- [6] D. Polarski and A. A. Starobinsky, Phys. Lett. B **356**, 196 (1995) doi:10.1016/0370-2693(95)00842-9 [astro-ph/9505125].
- [7] J. Garcia-Bellido and D. Wands, Phys. Rev. D **52**, 6739 (1995) doi:10.1103/PhysRevD.52.6739 [gr-qc/9506050].
- [8] M. Sasaki and E. D. Stewart, Prog. Theor. Phys. **95**, 71 (1996) doi:10.1143/PTP.95.71 [astro-ph/9507001].

- [9] V. F. Mukhanov, H. A. Feldman and R. H. Brandenberger, Phys. Rept. **215**, 203 (1992). doi:10.1016/0370-1573(92)90044-Z
- [10] A. R. Liddle and D. H. Lyth, Phys. Rept. **231**, 1 (1993) doi:10.1016/0370-1573(93)90114-S [astro-ph/9303019].
- [11] J. E. Lidsey, A. R. Liddle, E. W. Kolb, E. J. Copeland, T. Barreiro and M. Abney, Rev. Mod. Phys. **69**, 373 (1997) doi:10.1103/RevModPhys.69.373 [astro-ph/9508078].
- [12] A. R. Liddle, P. Parsons and J. D. Barrow, Phys. Rev. D **50**, 7222 (1994) doi:10.1103/PhysRevD.50.7222 [astro-ph/9408015].
- [13] N. C. Tsamis and R. P. Woodard, Annals Phys. **267**, 145 (1998) doi:10.1006/aphy.1998.5816 [hep-ph/9712331].
- [14] T. D. Saini, S. Raychaudhury, V. Sahni and A. A. Starobinsky, Phys. Rev. Lett. **85**, 1162 (2000) doi:10.1103/PhysRevLett.85.1162 [astro-ph/9910231].
- [15] S. Nojiri and S. D. Odintsov, Gen. Rel. Grav. **38**, 1285 (2006) doi:10.1007/s10714-006-0301-6 [hep-th/0506212].
- [16] R. P. Woodard, Lect. Notes Phys. **720**, 403 (2007) doi:10.1007/978-3-540-71013-4_14 [astro-ph/0601672].
- [17] Z. K. Guo, N. Ohta and Y. Z. Zhang, Mod. Phys. Lett. A **22**, 883 (2007) doi:10.1142/S0217732307022839 [astro-ph/0603109].
- [18] D. J. Brooker, N. C. Tsamis and R. P. Woodard, Phys. Rev. D **93**, no. 4, 043503 (2016) doi:10.1103/PhysRevD.93.043503 [arXiv:1507.07452 [astro-ph.CO]].
- [19] D. J. Brooker, N. C. Tsamis and R. P. Woodard, arXiv:1605.02729 [gr-qc].
- [20] M. G. Romania, N. C. Tsamis and R. P. Woodard, JCAP **1208**, 029 (2012) doi:10.1088/1475-7516/2012/08/029 [arXiv:1207.3227 [astro-ph.CO]].
- [21] D. J. Brooker, N. C. Tsamis and R. P. Woodard, arXiv:1603.06399 [astro-ph.CO].

- [22] D. J. Brooker, S. D. Odintsov and R. P. Woodard, Nucl. Phys. B **911**, 318 (2016) doi:10.1016/j.nuclphysb.2016.08.010 [arXiv:1606.05879 [gr-qc]].
- [23] R. P. Woodard, Int. J. Mod. Phys. D **23**, no. 09, 1430020 (2014) doi:10.1142/S0218271814300201 [arXiv:1407.4748 [gr-qc]].
- [24] P. A. R. Ade *et al.* [BICEP2 and Planck Collaborations], Phys. Rev. Lett. **114**, 101301 (2015) doi:10.1103/PhysRevLett.114.101301 [arXiv:1502.00612 [astro-ph.CO]].
- [25] P. A. R. Ade *et al.* [Planck Collaboration], Astron. Astrophys. **594**, A13 (2016) doi:10.1051/0004-6361/201525830 [arXiv:1502.01589 [astro-ph.CO]].
- [26] P. A. R. Ade *et al.* [Planck Collaboration], arXiv:1502.02114 [astro-ph.CO].
- [27] L. Covi, J. Hamann, A. Melchiorri, A. Slosar and I. Sorbera, Phys. Rev. D **74**, 083509 (2006) doi:10.1103/PhysRevD.74.083509 [astro-ph/0606452].
- [28] J. A. Adams, B. Cresswell and R. Easther, Phys. Rev. D **64**, 123514 (2001) doi:10.1103/PhysRevD.64.123514 [astro-ph/0102236].
- [29] M. J. Mortonson, C. Dvorkin, H. V. Peiris and W. Hu, Phys. Rev. D **79**, 103519 (2009) doi:10.1103/PhysRevD.79.103519 [arXiv:0903.4920 [astro-ph.CO]].
- [30] J. Hamann, L. Covi, A. Melchiorri and A. Slosar, Phys. Rev. D **76**, 023503 (2007) doi:10.1103/PhysRevD.76.023503 [astro-ph/0701380].
- [31] D. K. Hazra, A. Shafieloo, G. F. Smoot and A. A. Starobinsky, JCAP **1408**, 048 (2014) doi:10.1088/1475-7516/2014/08/048 [arXiv:1405.2012 [astro-ph.CO]].
- [32] D. K. Hazra, A. Shafieloo, G. F. Smoot and A. A. Starobinsky, JCAP **1609**, no. 09, 009 (2016) doi:10.1088/1475-7516/2016/09/009 [arXiv:1605.02106 [astro-ph.CO]].
- [33] K. Kadota, S. Dodelson, W. Hu and E. D. Stewart, Phys. Rev. D **72**, 023510 (2005) doi:10.1103/PhysRevD.72.023510 [astro-ph/0505158].

- [34] J. D. Barrow and A. Paliathanasis, arXiv:1611.06680 [gr-qc].
- [35] J. Mastache, F. Zago and A. Kosowsky, Phys. Rev. D **95**, no. 6, 063511 (2017) doi:10.1103/PhysRevD.95.063511 [arXiv:1611.03957 [astro-ph.CO]].
- [36] A. Achcarro, J. O. Gong, G. A. Palma and S. P. Patil, Phys. Rev. D **87**, no. 12, 121301 (2013) doi:10.1103/PhysRevD.87.121301 [arXiv:1211.5619 [astro-ph.CO]].
- [37] J. Torrado, B. Hu and A. Achucarro, arXiv:1611.10350 [astro-ph.CO].